Experimental Investigation of Frequency Domain Channel Extrapolation in Massive MIMO Systems for Zero-Feedback FDD

Thomas Choi, *Student Member, IEEE,* François Rottenberg, *Member, IEEE,* Jorge Gomez-Ponce, *Student Member, IEEE,* Akshay Ramesh, *Student Member, IEEE,* Peng Luo, *Student Member, IEEE,* Jianzhong Zhang, *Fellow, IEEE,* and Andreas F. Molisch, *Fellow, IEEE*

Abstract

Estimating the downlink channel state information (CSI) in the frequency division duplex (FDD) massive multi-input multi-output (MIMO) systems by means of the downlink pilots and the feedback requires an extra overhead which scales linearly with the copious number of antennas at the massive MIMO base station. To address this issue, this paper investigates the feasibility of the zero-feedback FDD massive MIMO systems based on channel extrapolation. The extrapolation uses high resolution parameter estimation (HRPE), specifically the space-alternating generalized expectation-maximization (SAGE) algorithm. HRPE is applied to two different channel models, vector spatial signature (VSS) and direction of arrival (DOA) models, to extract parameters of multipath components in the uplink channel and use these parameters to extrapolate the downlink CSI. These methods are evaluated by channel measurements using two separate channel sounder setups (switched array and virtual array), in two different environments (outdoor and indoor), in three microwave bands (2.4-2.5, 3.325-3.675, and 5-7 GHz). Performance metrics we evaluate include mean squared error, beamforming efficiency, and spectral efficiency in multi-user MIMO scenarios. The results show that extrapolation performs best

The work was supported by the NSF (ECCS-1731694), the Belgian National Science Foundation (FRS-FNRS), the Belgian American Educational Foundation, and Samsung Research America. A part of this article was presented in VTC2019-Fall [1].

T. Choi, J. Gomez-Ponce, A. Ramesh, P. Luo, and A. F. Molisch are with Ming Hsieh Department of Electrical and Computer Engineering, University of Southern California, Los Angeles, CA, USA. F. Rottenberg is with the Université catholique de Louvain, Louvain-la-Neuve, Belgium and the Université libre de Bruxelles, Brussels, Belgium. J. Zhang is with Samsung Research America, Richardson, TX, USA. Corresponding author: Thomas Choi (choit@usc.edu).

under the VSS model, without requiring antenna calibration, if the base station is in an open outdoor environment having line-of-sight paths to well separated users.

Index Terms

Zero-feedback FDD massive MIMO, channel extrapolation, high resolution parameter estimation, channel measurement, channel sounder, beamforming, multi-user MIMO

I. Introduction

A. Motivation and Problem Statement

Massive multiple-input multiple-output (MIMO) systems utilize tens to hundreds of antennas at the base station (BS) to increase spectral and energy efficiency of wireless networks, making them a promising solution for the challenges of rapidly growing numbers of wireless devices and soaring data capacity requirements [2]–[4]. Massive MIMO systems are generally assumed to operate in the time division duplexing (TDD) mode, where both the uplink and the downlink share the same frequency band[1] [5], [6]. This allows to exploit channel reciprocity to attain the downlink channel state information (CSI) using only the uplink pilots[2].

In the frequency division duplex (FDD) operation, the uplink and the downlink frequency bands are separated. Because the channel coherence bandwidth is almost always much smaller than the frequency spacing between the uplink and the downlink band, channel reciprocity cannot be directly exploited for the FDD operation. Therefore, extra overheads such as the downlink pilots and the feedback are necessary to attain the downlink CSI during the FDD operation. In addition, these overheads usually scale with the number of antennas at the BS rather than with the total number of the user equipment (UE) antennas, as is the case for the TDD. Consequently, overhead in the FDD might become prohibitive.

While such high resource demands from the FDD operation suggests massive MIMO systems to employ the optimal TDD operation, many legacy wireless networks still operate in the FDD frequency spectrum [7]. Therefore, the FDD massive MIMO systems can reduce costs from modifying hardware, frequency allocations, and/or network operation when updating current BSs with small number of antennas to massive MIMO BSs. For this reason, extrapolation of

[1]In fact, several researchers “define” massive MIMO to operate in the TDD by default [4].

[2]Reciprocity assumption only holds when both the uplink and the downlink occur within the channel coherence time - usually in scales of milliseconds.

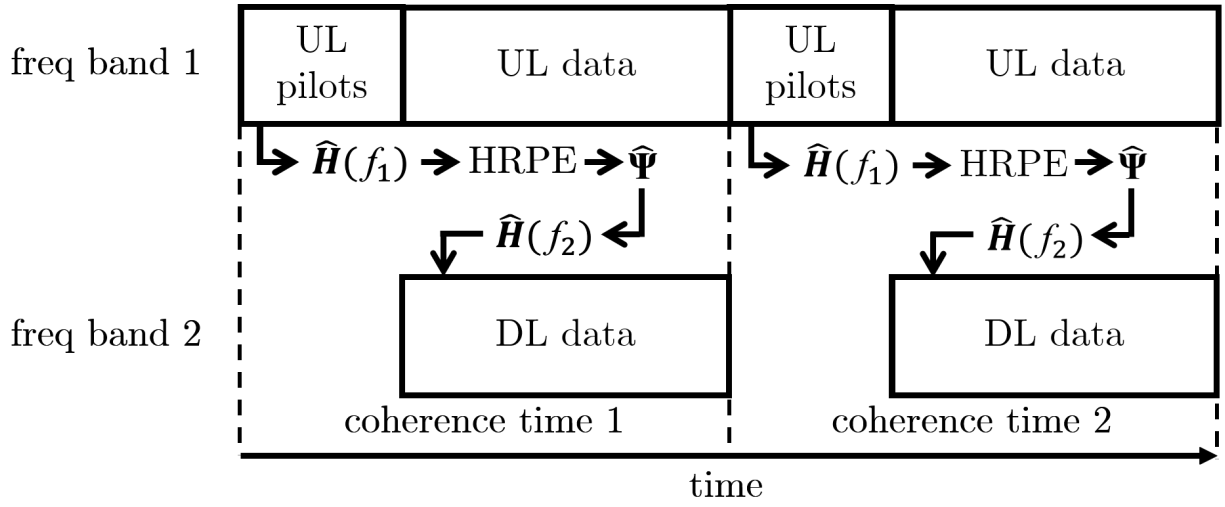

Fig. 1. Proposed zero-feedback FDD massive MIMO operation based on HRPE

channels in the frequency domain have drawn considerable attention (see Sec. I-C for a literature review). In particular, in [8], [9], we investigated theoretically an approach in which channel extrapolation is done based on high resolution parameter estimation (HRPE) of the multipath components (MPCs). More precisely, the transfer function of a wireless channel is the complex sum of the contributions of the individual MPCs. A HRPE algorithm determines the parameters of each MPC such as complex amplitude, delay, azimuth angle of arrival, and elevation angle of arrival, from the uplink channel measurements. Based on these results, one can synthesize the channel in the downlink frequency band. Assuming that the parameters of each MPC in the downlink channel are the same as in the uplink channel, the downlink CSI can be estimated, without any downlink pilots or feedback to resolve resource issue in the FDD massive MIMO systems (see Fig. 1).

B. Contributions

1) In this paper, we apply the framework of [9] to extensive measurement results and evaluate the performance. The selected HRPE algorithm is the space-alternating generalized expectation-maximization (SAGE) algorithm, used in two variations based on the vector spatial signature (VSS) model [10] and the direction of arrival (DOA) model [11], forming separate sets of parameters for MPCs.

2) Multiple channel measurements have been conducted using two massive MIMO channel sounder setups (switched array and virtual array), in two different types of environment (outdoor and indoor), in three different microwave bands (2.4-2.5, 3.325-3.675, and 5-7 GHz) to assess the performance of the proposed channel extrapolation method without being biased toward certain measurement settings. The “measured channel (considered as ground truth channel in this paper) at the downlink frequency band” was compared with “estimated channel at the downlink frequency band”, constructed by channel extrapolation using parameters of MPCs obtained purely from “measured channel at the uplink frequency band”. This uplink frequency band in the FDD massive MIMO is also called a training band in channel extrapolation, which is a frequency band used for attaining parameters of MPCs to estimate channels at the other frequency bands, such as the downlink frequency band in the FDD massive MIMO.
3) Three different metrics assess the evaluated "accuracy" of the estimated downlink channel in comparison to the ground truth downlink channel, and the expected “performance” of the FDD massive MIMO systems using the estimated downlink channel. These metrics include mean squared error (MSE) of the channel estimate, beamforming efficiency, and spectral efficiency in multi-user MIMO scenarios. Overall, these metrics investigate the feasibility of the zero-feedback FDD massive MIMO systems using channel extrapolation based on HRPE algorithms.

This paper makes several assumptions and acknowledges limitations in the following:

1) Implementing the proposed channel extrapolation method for the actual FDD massive MIMO systems in practice could be challenging due to computational complexity of HRPE algorithms. Rather, the emphasis in this paper is on the performance evaluation and the feasibility study of high-accuracy algorithms. There are several ways to speed up the MPC extraction using HRPE algorithm, but accuracy will be traded off by reducing the total number of MPCs, number of iterations, resolutions of parameters, etc. The performance resulting from such trade-offs is not studied in this paper.
2) While the switched array setup captures the channel within several milliseconds, a virtual array takes several seconds or minutes to record the channel. Therefore, virtual arrays were used for indoor scenarios with static environment while a switched array was used for outdoor scenarios. For the multi-user studies, we postulate that measurements with

a single UE at different times is equivalent to measurement with multiple UEs at the same time, which is true only if the environment is completely static. Yet, for outdoor measurements, movement of scattering objects during the time it took to move physically the antenna from one location to the next might have occurred. We tried to minimize the effects of moving environmental objects, but quantitative assessment of the residual effects is not possible.

C. Literature Review

1) Theoretical studies of the FDD massive MIMO: There are several previous works that studied the feasibility of the FDD massive MIMO with reduced overhead. Among the suggested approaches are compressive sensing (CS) [12], using long term channel statistics and previous signals in a closed-loop manner [13], or a combination thereof [14]. There were also other potential solutions for the FDD massive MIMO systems to reduce or remove extra overheads, which utilize spatial correlation between multiple users [15], [16], spatial basis expansion model based on array theory [17], reciprocity based on reverse training [18], small number of dominant angles-of-departure [19], and deep learning [20]–[22].

There were also studies like this paper which used HRPE algorithms. One study used MUSIC and ESPIRIT to model channels in disjoint frequency bands [23]. In [24] and [25], the authors show that high resolution algorithms/MPC extractions are more suited than compressive sensing to exploit the FDD channel reciprocity. However, these papers did not verify the proposed performance empirically in real world channels.

2) Empirical Studies of the FDD massive MIMO: There were also several measurement-based studies which analyzed performance of the FDD massive MIMO systems (summarized in Table I). Ref. [6] showed that the reciprocity-based TDD massive MIMO performs better than the feedback-based FDD massive MIMO with predetermined grid of beams, especially in non-line-of-sight (NLOS) cases, based on channel measurements at 2.6 GHz carrier frequency and 50 MHz bandwidth. In [26], in order to reduce the overheads, authors used the downlink training and the feedback only toward four dominant directions, showing improvement of spectral efficiency by 150% in comparison to the full training and the feedback. The measurements were conducted with 64 antennas at 2.4 GHz, with 20 MHz training band for estimation and 72 MHz uplink and downlink band separation.

TABLE I

LIST OF THE EMPIRICAL FDD MASSIVE MIMO RESEARCH

Institution	DL CSI selection/estimation method	Feedback
Lund [6]	choose best beam among grid of beams	yes
Rice [26]	maximum likelihood method [27] for dominant DoAs	yes
Ericsson [28]	modified maximum likelihood method [29]	no
MIT [30]	R2-F2 [30]	no
Stuttgart [31]	deep learning	no
USC	SAGE VSS [10] / DOA [11]	no

Several papers experimentally investigated zero-feedback methods for the FDD massive MIMO. Ref. [28] used 8×8 MIMO measurements and a modified maximum likelihood estimator to investigate extrapolation performance in the spatial and the frequency domain, using 5 MHz training band within 2.4-2.45 GHz. Ref. [30], employed the R2-F2 method, which utilizes phase changes from inter-antenna separation at the BS to estimate the channel at another frequency band, showing low loss in beamforming performance of the FDD system with the estimated channels in comparison to the ground truth channels. The setup used five antennas at the BS, using 10 MHz training band within the 640-690 MHz band. Another zero-feedback method includes applying deep learning, using a large amount of training data to predict the downlink channel based on the uplink channel [31]. The setup used 32 antennas at the base station with 20 MHz training band and 25 MHz uplink and downlink band separation within the 1.2-1.3 GHz band.

As mentioned in section 1-B, this paper is different from other papers as HRPE algorithm based on the VSS and the DOA models are used on the uplink channel to estimate the downlink channel without the extra overheads. We showed a theoretical analysis based on the DOA model in [8], [9], and initial outdoor measurement results in our conference paper [1]. The current paper expands our previous results by 1) comparing with another channel model (VSS) for the HRPE evaluation and extrapolation that has the advantage of not requiring pattern calibration, 2) using measurement settings including more locations and different (virtual array) setups, and 3) employing an additional figure of merit (spectral efficiency) for multi-user massive MIMO systems. The measurement setups include 64 antenna elements cylindrical switched array at

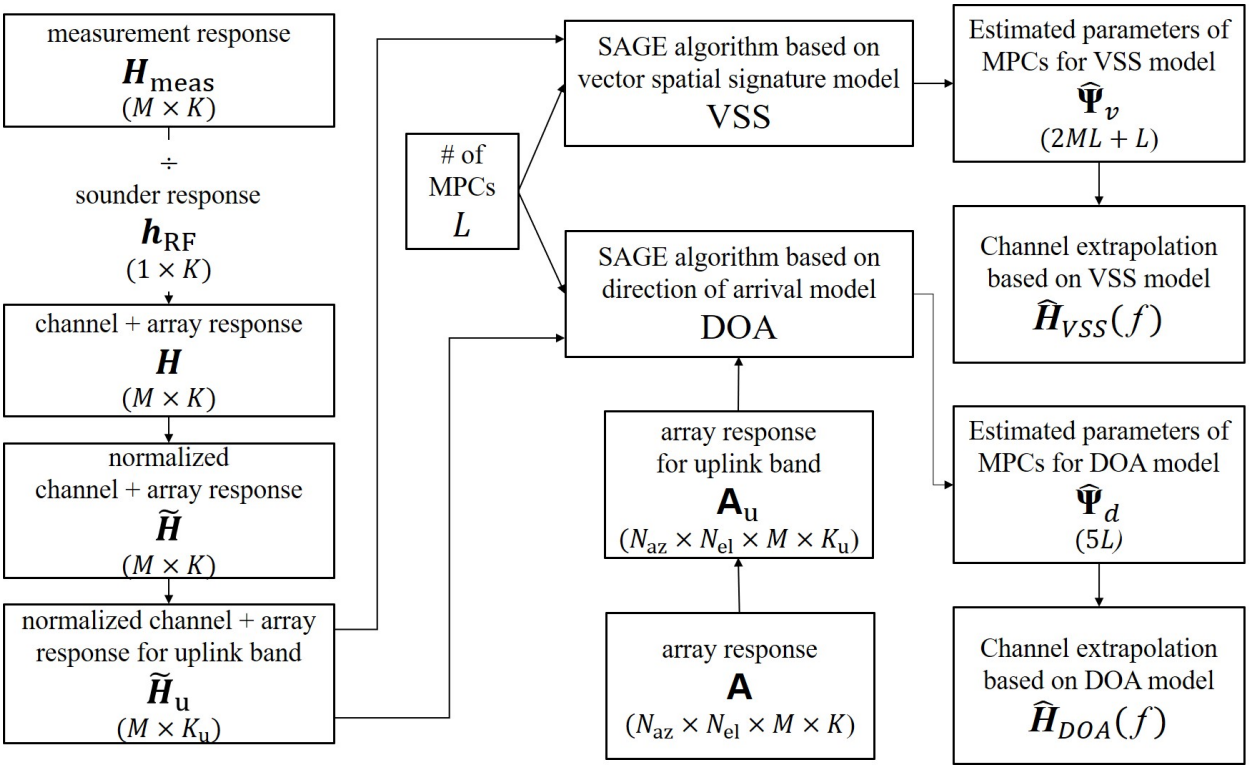

Fig. 2. Detailed process of channel extrapolation using the SAGE algorithm based on the VSS and the DOA models

3.325-3.675 GHz using 35 MHz training band [1], 90 positions virtual array at 2.4-2.5 GHz with 20 MHz training band, and 72 positions virtual array at 5-7 GHz with 50 MHz training band. More recently, [32] used a similar channel inference method using the SAGE and four different types of calibration methods. However, only a DOA model excluding elevation angle of arrival was used, measurements were conducted with smaller bandwidth at less locations, and multi-user scenarios were not considered.

II. VSS and DOA Channel Models

In this work, we consider parametric channel models to 1) estimate the path parameters using an HRPE algorithm to get complete descriptions of the channels and 2) extrapolate CSI to the other frequency bands using the parameters obtained from the training band. The overall inputs and outputs of HRPE algorithms depending on two different models are shown in Fig. 2, which will be explained in the following subsections.

A. Channel Matrix for HRPE Algorithm

HRPE algorithms takes complex channel data as an input, producing parameter values for MPCs that are applied to channel models. The structure and processing of the measured channel data are described in this subsection (details of measurements are further discussed in Section IV).

First, raw channel data measured by the receiver of a channel sounder, $\boldsymbol{H}_{\text{meas}}$, with dimension $M \times K$ are selected, where M is the number of antennas at the BS and K is the number of frequency samples of the measurement. Subscript *meas* indicates that the data has not yet been compensated for the response of the RF system, $\boldsymbol{h}_{\text{RF}}$.[3] $\boldsymbol{h}_{\text{RF}}$ can be measured by the back-to-back calibration of the sounder transmitter (TX) and receiver (RX), connected by a cable connection. The compensated frequency response of the channel and the antennas only, $\boldsymbol{H}$, is attained by

$$\boldsymbol{H} = \boldsymbol{H}_{\text{meas}} \cdot \begin{bmatrix} {h_{\text{RF},1}}^{-1} & 0 & \cdots & 0 \\ 0 & {h_{\text{RF},2}}^{-1} & \cdots & 0 \\ \vdots & \vdots & \ddots & \vdots \\ 0 & 0 & \cdots & {h_{\text{RF},K}}^{-1} \end{bmatrix} \tag{1}$$

where ${h_{\text{RF},k}}^{-1}$ represents the inverse of the RF system frequency response at kth frequency index. If the averaged power of $\boldsymbol{H}$ is expressed as ${\mu_{\boldsymbol{H}}}^2 = \frac{||\boldsymbol{H}||_F^2}{MK}$ where $||\cdot||_F$ is the Frobenius norm, then the normalized channel measurement matrix $\tilde{\boldsymbol{H}} = \frac{\boldsymbol{H}}{\mu_{\boldsymbol{H}}}$. Among $\tilde{\boldsymbol{H}}$ with dimension of $M \times K$, a subset which represents channel measurement data of the uplink frequency band, $\tilde{\boldsymbol{H}}_{\text{u}}$, is selected, with dimension $M \times K_{\text{u}}$. $\tilde{\boldsymbol{H}}_{\text{u}}$ becomes the input for HRPE algorithm.

While there are many well-known HRPE algorithms such as MUSIC [33], ESPRIT [34], CLEAN [35], and RiMAX [36], SAGE was selected. The choice of HRPE algorithm was arbitrary, as the extrapolation results were dependent on channel models rather than types of HRPE algorithms during preliminary analysis. Two channel models (VSS and DOA) were used to attain different types and values of path parameters, which are discussed in the following subsections. A more detailed description of the SAGE algorithm are given in Appendix A.

[3] $\boldsymbol{h}_{\text{RF}}$ is a one dimensional frequency response because the switched array setup we used relies on a single RF chain for all antennas - it can be a matrix for other setups if multiple RF chains are used. This notation must not be confused as the impulse response notation which usually employs lower case letter.

B. Vector Spatial Signature (VSS) Model

The main difference between the VSS and the DOA models is that the VSS model does not require calibrated array pattern, $\mathbf{A}$, as it does not estimate angles of arrival of MPCs. The only input for the VSS algorithm other than the normalized channel measurement data at the uplink frequency band, $\tilde{\boldsymbol{H}}_{\mathrm{u}}$, is L, the number of MPCs (Fig. 2). L is arbitrarily chosen because the actual number of MPCs is not known. While using a very large number can improve the performance within the selected bandwidth for SAGE evaluations, it may lead to overfitting and channel extrapolation usually performs worse outside the training bandwidth during channel extrapolation [1].

The first parameter of the VSS model is estimated delay, $\hat{\tau}_v$, where v is the index of MPC. The second parameter is called "vector spatial signature", represented by $\hat{\mathbf{a}}_v$. $\hat{\mathbf{a}}_v$ is a *frequency independent* complex vector with size $M \times 1$ which according to [10], is "not explicit functions of angles of arrival, but instead *abstractly* represent the response of the array pattern for path v with delay τ_v". The extrapolation range is limited for the VSS model because in practice, most array patterns are frequency dependent. However, the estimation within the training band will be very accurate for massive MIMO systems because the number of estimated parameters in vector spatial signatures scales with M; more parameters can be adjusted to best estimate the channel response. Also, the VSS model does not suffer from calibration errors since it does not rely on calibration. The VSS channel model is overall expressed as:

$$\hat{\boldsymbol{H}}_{VSS}(f) = \sum_{v=1}^{L} \hat{\mathbf{a}}_{\boldsymbol{v}} e^{-2\pi f \hat{\tau}_v}. \tag{2}$$

Once both $\hat{\mathbf{a}}_v$ and τ_v are estimated for all L paths from the training frequency band, CSI at the desired frequency, f_{d}, can be attained by setting $f = f_{\mathrm{d}}$ in eq. (2), where f_{d} will be within the downlink frequency band. The physical meaning of the VSS model is that only phase changes with frequency.

In total, $2ML + L$ real-valued parameters are estimated by the VSS model, where $2ML$ comes from real and imaginary values of the vector spatial signatures for all antennas for all paths, and L represents the total number of delays.

C. Direction of Arrival (DOA) Model

As the name indicates, the DOA model requires a frequency dependent calibrated antenna array pattern, $\mathbf{A}$, to determine the directions of incoming MPCs. Aside from the topic of channel extrapolation, this model is useful when angular information of the channel is needed. Like the VSS model, the DOA model also requires normalized channel measurement data in the uplink frequency band, $\tilde{\boldsymbol{H}}_{\mathrm{u}}$, and the total number of MPCs, L (Fig. 2).

$\mathbf{A}$ is attained differently for a switched array and a virtual array [1]. For a switched array, a reference antenna with a known pattern is positioned on one side of anechoic chamber and the switched array is positioned on another side, supported by a rotating positioner. The array rotates to a certain azimuth and elevation position, switches on a selected antenna element, and a vector network analyzer (VNA) sweeps across the frequency to record the channel frequency response. Then, the next antenna element is turned on for another VNA sweep. After obtaining the transfer function for each antenna element, the antenna array rotates to a new azimuth and elevation position and repeats the process to record the channel frequency response at the selected position. At the end, 4-D calibration data with size of $N_{\mathrm{az}} \times N_{\mathrm{el}} \times M \times K$ is created, where N_{az} and N_{el} are the number of azimuth steps and number of elevation steps during calibration. The calibrated antenna pattern for the subset of the uplink frequency band, $\mathbf{A}_{\mathrm{u}}$, is selected as an input for HRPE algorithm, with size of $N_{\mathrm{az}} \times N_{\mathrm{el}} \times M \times K_{\mathrm{u}}$. The rest of the calibration data will be used during the channel extrapolation to the frequency in the downlink band.

Virtual array calibration, however, omits switching, so a 3-D calibration data of a single antenna with dimension $N_{\mathrm{az}} \times N_{\mathrm{el}} \times K$ will be created first. This 3-D calibration data of a single antenna will then be rotated or moved M times to form a 4-D calibration data of a virtual antenna array with selected geometrical shape and numbers. The impact of the rotation/movement is computed geometrically, not measured explicitly. The formulated calibration data, $\mathbf{A}$, with the dimension $N_{\mathrm{az}} \times N_{\mathrm{el}} \times M \times K$, are then used in the same way as the switched-array calibration data.

In [1], [9], we have already shown output parameters of MPCs attained by the SAGE algorithm based on the DOA model and channel extrapolation results in an anechoic chamber and some locations outdoors. The estimated parameters for each MPC in a single-input multi-output (SIMO) channel included complex amplitude, $\hat{\alpha}$, delay, $\hat{\tau}$, azimuth angle of arrival $\hat{\phi}$, and elevation angle of arrival $\hat{\theta}$. The estimated parameters of the same DOA model used here added subscript d ($\hat{\alpha}_d$, $\hat{\tau}_d$, $\hat{\phi}_d$, and $\hat{\theta}_d$) as an index of MPC to distinguish between parameters of the VSS

TABLE II

ESTIMATED PARAMETERS OF MPCS FOR THE VSS AND THE DOA CHANNEL MODELS

Model	Estimated parameters of MPCs	Channel model
VSS	$\hat{\boldsymbol{\psi}}_v = [\hat{\mathbf{a}}_v, \hat{\tau}_v]$	$\hat{\boldsymbol{H}}_{VSS}(f) = \sum_{v=1}^{L} \hat{\mathbf{a}}_{\boldsymbol{v}} e^{-2\pi f \hat{\tau}_v}$
DOA	$\hat{\boldsymbol{\psi}}_d = [\hat{\alpha}_d, \hat{\tau}_d, \hat{\phi}_d, \hat{\theta}_d]$	$\hat{\boldsymbol{H}}_{DOA}(f) = \sum_{d=1}^{L} \hat{\alpha}_d \mathbf{A}(\hat{\phi}_d, \hat{\theta}_d, f) e^{-2\pi f \hat{\tau}_d}$

and the DOA models. These parameters are summarized in Table II. There are $5L$ parameters to estimate for L paths, which are much less than the VSS model's $2ML + L$ parameters.

After parameters are estimated from the uplink frequency band, they are plugged into the channel model to estimate the channel frequency response at any selected frequency f. The DOA channel model is:

$$\hat{\boldsymbol{H}}_{DOA}(f) = \sum_{d=1}^{L} \hat{\alpha}_d \mathbf{A}(\hat{\phi}_d, \hat{\theta}_d, f) e^{-2\pi f \hat{\tau}_d}, \tag{3}$$

where $\mathbf{A}(\hat{\phi}_d, \hat{\theta}_d, f)$ is the one dimensional ($M \times 1$) slice of four dimensional antenna array response over M antenna elements or positions, dependent on the estimated azimuth angle of arrival from the uplink band, the estimated elevation angle of arrival from the uplink band, and the frequency of choice. The array pattern at a specific frequency is obtained, either through including the frequency point during calibration or through interpolation if the desired frequency is between two measured frequency points during calibration. The physical meaning is that both the antenna response and the exponential term indicate phase change with frequency.

III. PERFORMANCE METRICS

Three different types of performance metrics are selected to assess the performance of the extrapolation algorithms: mean squared error (MSE) of the channel estimates, beamforming efficiency, and spectral efficiency for multi-user scenarios.

A. Mean Squared Error (MSE) of the Channel Estimates

MSE averages the squared magnitude of the differences between normalized complex channel response of a measured (ground truth) channel and an estimated channel at the selected frequency over all antennas:

$$MSE(f) \triangleq \frac{||\tilde{\boldsymbol{H}}(f) - \hat{\boldsymbol{H}}(f)||_2^2}{M} \tag{4}$$

where $\hat{\boldsymbol{H}}(f)$ can be either $\hat{\boldsymbol{H}}_{DOA}(f)$ or $\hat{\boldsymbol{H}}_{VSS}(f)$ with dimension $M \times 1$ and $||\cdot||_2$ is the Euclidean norm. If f lies within the training band (e.g. the uplink band in the FDD massive MIMO systems), then MSE will be a measure of the interpolation performance. If f lies outside the training band (e.g. the downlink band in the FDD massive MIMO systems), then MSE will be a measure of extrapolation performance. In the results in later section, MSE will be represented on a dB scale.

B. Beamforming Efficiency

Massive MIMO array can give a beamforming gain by combining constructive contributions of the many antenna elements within the array. One common way to optimize beamforming gain (in single-user case) is in the form of maximum-ratio combining, by using matched filtering based on estimated channel response. Beamforming efficiency indicates how beamforming gain with estimated CSI compares with beamforming gain based on perfect CSI, based on an assumption that the measured CSI is the perfect CSI. Beamforming gain (BG) with perfect CSI, estimated CSI, and uniform beamforming are expressed as:

$$BG_{perfect}(f) \triangleq ||\tilde{\boldsymbol{H}}(f)||_2^2 \tag{5}$$

$$BG_{estimated}(f) \triangleq \frac{|\hat{\boldsymbol{H}}(f)^{\dagger}\tilde{\boldsymbol{H}}(f)|^2}{||\hat{\boldsymbol{H}}(f)||_2^2} \tag{6}$$

$$BG_{uniform}(f) \triangleq \frac{||\tilde{\boldsymbol{H}}(f)||_2^2}{M} \tag{7}$$

where † is the conjugate transpose operator. Therefore, using eq. (5) and (6), beamforming efficiency (BE) is:

$$BE(f) \triangleq \frac{|\hat{\boldsymbol{H}}(f)^{\dagger}\tilde{\boldsymbol{H}}(f)|^2}{||\hat{\boldsymbol{H}}(f)||_2^2||\tilde{\boldsymbol{H}}(f)||_2^2} \tag{8}$$

and this value ranges from 0 to 1 with 1 indicating full efficiency. As in the case of MSE, beamforming efficiency will be represented on a dB scale in later discussions.

C. Spectral Efficiency in Multi-User MIMO Systems

Earlier metrics were based on a single-user assumption. Spectral efficiency for every UE in a multi-user MIMO system can be determined by SIMO measurements at multiple locations. Spectral efficiency of the UE n at the frequency f is represented as:

$$C^{(n)}(f) = log_2(1 + SINR^{(n)}(f))\ (bits/s/Hz), \tag{9}$$

where SINR(f) is a signal-to-interference-plus-noise ratio at a given frequency and the index of each UE, n, varies from 1 to N. The received signal by the n-th UE at frequency f during the downlink phase is:

$$r^{(n)}(f) = \boldsymbol{H}^{(n)}(f)^{\mathsf{T}}\tilde{\boldsymbol{G}}^{(n)}(f)s^{(n)} + \sum_{n' \neq n}^{N} \boldsymbol{H}^{(n)}(f)^{\mathsf{T}}\tilde{\boldsymbol{G}}^{(n')}(f)s^{(n')} + w^{(n)}, \tag{10}$$

where T is a transpose operator, $r^{(n)}(f)$ is a complex value received by the UE at the selected frequency, f, $\boldsymbol{H}^{(n)}(f)$ is a ground truth channel vector for the UE at the frequency f from every antenna with dimension $M \times 1$, $\tilde{\boldsymbol{G}}^{(n)}(f)$ is a normalized precoding vector for the UE at the frequency f from every antenna with dimension $M \times 1$, $s^{(n)}$ is a transmitted signal from the BS for the UE, and $w^{(n)}$ is a noise received by the UE. The first term indicates the beamforming signal for the UE n while the second term indicates the interference from the signals intended for other UEs received by the UE n. Therefore, $SINR^{(n)}(f)$ can be calculated as:

$$SINR^{(n)}(f) = \frac{|\boldsymbol{H}^{(n)}(f)^{\mathsf{T}}\tilde{\boldsymbol{G}}^{(n)}(f)|^2 {\sigma_{s^{(n)}}}^2}{\sum_{n' \neq n}^{N} |\boldsymbol{H}^{(n)}(f)^{\mathsf{T}}\tilde{\boldsymbol{G}}^{(n')}(f)|^2 {\sigma_{s^{(n')}}}^2 + {\sigma_{w^{(n)}}}^2} \tag{11}$$

where ${\sigma_{s^{(n)}}}^2$ and ${\sigma_{w^{(n)}}}^2$ are variances of the signal and the noise, assumed to be the same for all N UEs (i.e., all UEs are expected to experience the same transmit power from BS and same noise power).

The normalized precoding vector, $\tilde{\boldsymbol{G}}^{(n)}(f)$, can be created as follows. First,

$$\hat{\boldsymbol{H}}_{MU}(f) = [\hat{\boldsymbol{H}}^{(1)}(f), \hat{\boldsymbol{H}}^{(2)}(f), ..., \hat{\boldsymbol{H}}^{(N)}(f)] = \begin{bmatrix} \hat{H}_1^{(1)}(f) & \hat{H}_1^{(2)}(f) & \cdots & \hat{H}_1^{(N)}(f) \\ \hat{H}_2^{(1)}(f) & \hat{H}_2^{(2)}(f) & \cdots & \hat{H}_2^{(N)}(f) \\ \vdots & \vdots & \ddots & \vdots \\ \hat{H}_M^{(1)}(f) & \hat{H}_M^{(2)}(f) & \cdots & \hat{H}_M^{(N)}(f) \end{bmatrix}$$

where $\hat{H}_m^{(n)}(f)$ represents an estimated complex channel frequency response between the BS antenna m and the UE n at the frequency f. Then, the precoding matrix for N UEs can be determined in two ways: maximum ratio (MR) and zero-forcing (ZF):

$$\boldsymbol{G}_{MR}(f) = \hat{\boldsymbol{H}}_{MU}(f)^{\dagger} \tag{12}$$

$$\boldsymbol{G}_{ZF}(f) = \hat{\boldsymbol{H}}_{MU}(f)^{\dagger}(\hat{\boldsymbol{H}}_{MU}(f)\hat{\boldsymbol{H}}_{MU}(f)^{\dagger})^{-1} \tag{13}$$

where dimension of both matrices is $N \times M$. $\boldsymbol{G}^{(n)}(f)$ is a precoding vector for UE n with size $M \times 1$ (transpose of row n of either $\boldsymbol{G}_{MR}(f)$ or $\boldsymbol{G}_{ZF}(f)$). Finally, we normalize this precoding vector to get normalized precoding vector per UE, $\tilde{\boldsymbol{G}}^{(n)}(f) = \frac{\boldsymbol{G}^{(n)}(f)}{||\boldsymbol{G}^{(n)}(f)||_2}$.

IV. Measurement Setups and Settings

Measurement campaigns were conducted using two types of channel sounders in different environments. For both channel sounders, an omnidirectional antenna was used at the TX emulating a UE. In order to consider the measured channel as the reference "ground truth" channel to compare with the estimated channel, high SNR was necessary during measurement. Therefore, transmitting power up to 40 dBm was used during outdoor measurements and up to 28 dBm during indoor measurements. On the BS side, the outdoor channel sounder setup used a switched array and the indoor channel sounder setup used a virtual array.

A. Outdoor Measurements with Switched Array

To measure channel characteristics of outdoor channels with short coherence time, a switched array with 64 antenna elements was used as a RX, emulating a massive MIMO base station (Fig. 3a). The antenna array is cylindrical, having 16 columns of 6×1 linear antenna array. Each antenna is a stacked patch antenna design, which increases beamwidth and bandwidth in comparison to conventional patch antennas. Because top and bottom antenna elements per each column are used as "dummy" antenna elements, 4 antenna elements per column are used during the measurement, resulting in 64 active antenna elements. There are two ports per antenna element, (vertical/horizontal polarization), but only vertically polarized ports are considered because vertically polarized antenna was used on TX. Radiation patterns of the antenna elements are also described in [1].

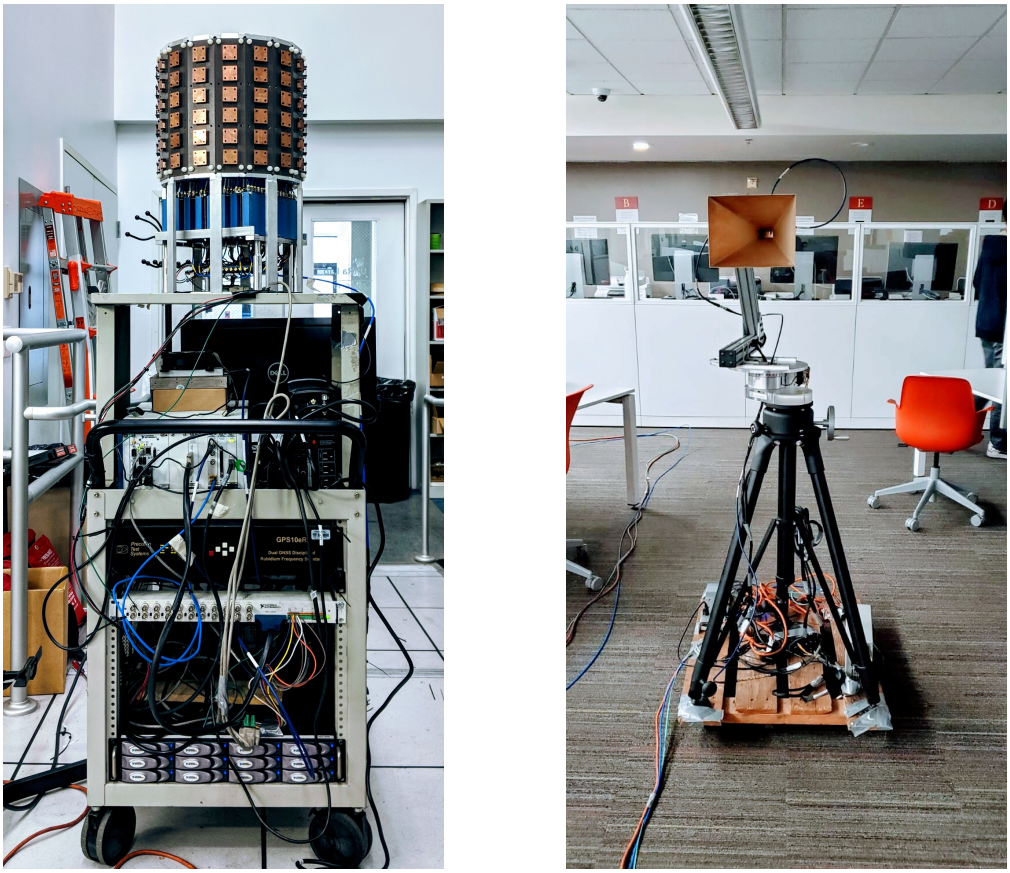

(a) Real time sounder with switched array

(b) VNA based sounder with rotating horn

Fig. 3. Two types of channel sounders used for measuring channel responses of dynamic outdoor and static indoor environments

These 64 active antenna elements are then connected to eight 16×1 switches, which are cascaded with one 8×1 switch, resulting in single RF chain at the RX. Single RF chain simplifies the RF "back-to-back" calibration as well as sounder operation. The switches are controlled with a digital control interface. The sounder captures channel responses across all 64 antenna elements in 10 milliseconds. This is smaller than the channel coherence time, since the only possible movement came from slow-moving objects such as people and leaves of the trees.

The sounder operates in the 3.5 GHz frequency range, with a measurement band from 3.325 to 3.675 GHz. It uses a multitone waveform with low crest factor [37] to achieve low peak to average power ratio (PAPR) that allows operation close to the 1 dB compression point of the power amplifier. The subcarrier spacing was 125 kHz, resulting in 2801 subcarriers within a 350 MHz measured bandwidth. Because the TX (arbitrary waveform generator) and the RX (digital oscilloscope) are physically separated during the measurement, they were synchronized

Fig. 4. Map of outdoor measurement campaigns: UEs with LOS paths are marked blue, UEs with trees blocking the LOS path are marked purple (obstructed LOS), and UEs with paths blocked by building are marked red (NLOS).

by two rubidium clocks disciplined by global positioning system (GPS) satellites for accurate delay estimation.

The outdoor measurements were conducted at the northeast side of the University of Southern California (USC) University Park Campus (see Fig. 4), where the BS was positioned on top of a four stories high parking structure. There were in total 12 UE locations and three cases (four UEs per case). The first case is a line-of-sight (LOS) case, where UEs were positioned close to the parking structure with LOS path available (marked in blue). The second case is an obstructed-line-of-sight (OLOS), where UEs were spread out through the quad further away from the parking structure with trees blocking the LOS path (marked in purple). The last case is a non-line-of-sight (NLOS) case, where UEs were surrounding the library with the LOS path blocked by building (marked in red).

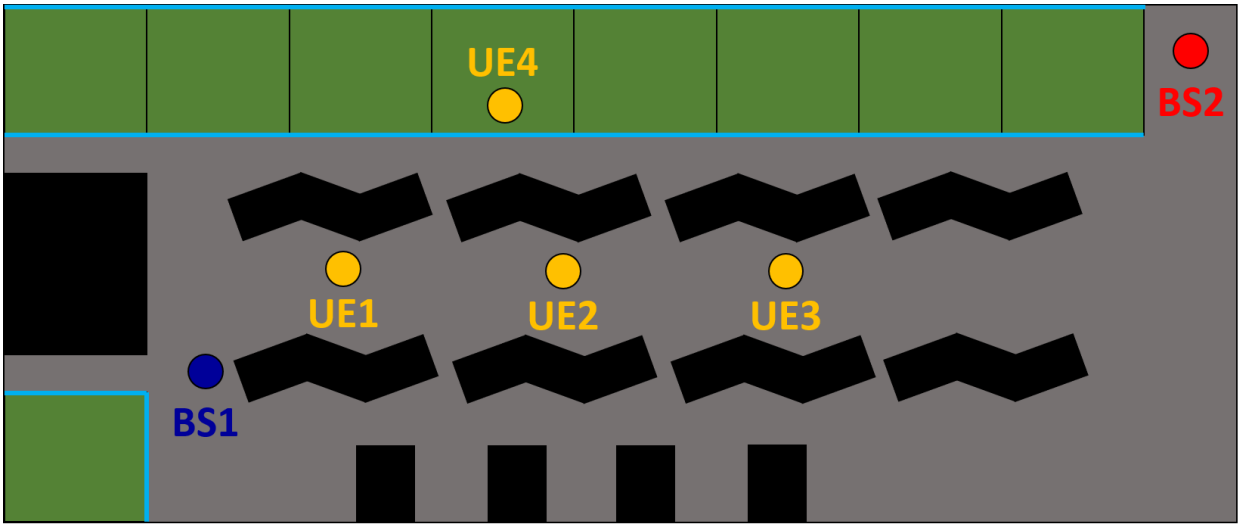

Fig. 5. Map of indoor measurement campaigns: Location of BS serving UEs at LOS paths is marked blue, another location of BS serving same UEs at NLOS paths is marked red, and 4 locations of UEs are marked in yellow. Tables are marked in black and small rooms are marked in green, where sky blue edges indicate glass doors and windows.

B. Indoor Measurements with Virtual Array

For the indoor measurements, a vector network analyzer (VNA) based channel sounder with a rotating horn antenna forming a virtual massive MIMO array (Fig. 3b) on the RX side was selected. While indoor channel characteristics can also be measured using the real time channel sounder with switched array, we opted for a different measurement method both to provide data with different setups. Also, the use of a precision VNA as TX and RX can result in higher accuracy, though its use is only feasible for measurements over short distances. Each measurement was conducted two times, at two frequency bands (2.4-2.5 GHz and 5-7 GHz).

When repeating measurement two times at two separate frequency bands, several setup configurations were altered including waveform, horn antenna, and number of antenna positions. 201 frequency points were used for 2.4-2.5 GHz band (500 kHz frequency spacing) and 1601 frequency points were used for 5-7 GHz band (1.25 MHz frequency spacing). Larger frequency spacing with respect to outdoor can be used because smaller excess delay is expected. The intermediate frequency (IF) bandwidth of the VNA was set to 500 kHz. The coarse frequency spacing and the wide IF bandwidth helped reduce the measurement time being significantly longer than the measurement time of the real time channel sounder. The total measurement time was 75 seconds for each of both 2.4-2.5 GHz and 5-7 GHz measurements per position.

In terms of antenna, two different horn antennas, both with 20 dBi gain, were used at the two frequency bands. The 3dB beamwidth of horn antenna used at 2.4 GHz was 12 degrees and that of the horn for 5-7 GHz band was 15 to 19 degrees, varying across the frequency. Therefore, azimuth was sampled every 12 degrees for 2.4 GHz, resulting in 30 azimuth points per elevation, and every 15 degrees for 5-7 GHz, resulting in 24 azimuth points per elevation. There were three elevation angles for both measurement setups, where the antenna was facing straight horizontally, 10 degrees down from the horizontal plane, and 10 degrees up from the horizontal plane. Total antenna positions per location were therefore $30 \times 3 = 90$ for 2.4-2.5 GHz and $24 \times 3 = 72$ for 5-7 GHz measurements.

Indoor measurements were conducted on the second floor of the Leavey Library at the USC (Fig. 5). The virtual array was put in two corners of the floor, while the omnidirectional antenna was moved to four different locations. The first BS (RX) location had LOS paths available from UEs (TX), while the second BS location had NLOS paths from UEs. The UE was positioned at 1.55m height while the BS was positioned at 2.47m height. The doors and the windows of the rooms were made of glass. During the measurement, all Wi-Fi access points on the floor were covered with absorbers to prevent interference.

V. Analysis of Results

A. 3.325-3.675 GHz Outdoor

First, 3.325-3.675 GHz outdoor measurements with switched array are analyzed. 35 MHz around the 3.5 GHz center frequency (3.4825-3.5175 GHz) was selected as a training band and the remaining 315 MHz are used for validation of extrapolation results. For each location, the SAGE algorithm was applied twice, based on the VSS and the DOA models. 10 paths were used for the VSS model and 40 paths were used for the DOA model, where the number of paths was increased until MSE < -10 dB within the training band. LOS (UE1 to UE4), OLOS (UE5 to UE8), and NLOS (UE9 to UE12) cases are analyzed separately.

In Fig. 6a and 6b, the MSE is shown, where the solid lines indicate the results based on the VSS model and the dash-dot lines indicate the results based on the DOA model. The blue lines evaluate UE 3 (LOS), the purple lines evaluate UE 6 (OLOS), and the red lines evaluate UE 12 (NLOS), where the sample UEs were chosen at random. The frequencies within the black dashed lines indicate the training band, while the frequencies outside the band are the frequencies for extrapolation. The graph clearly shows that within the training band, the SAGE algorithm

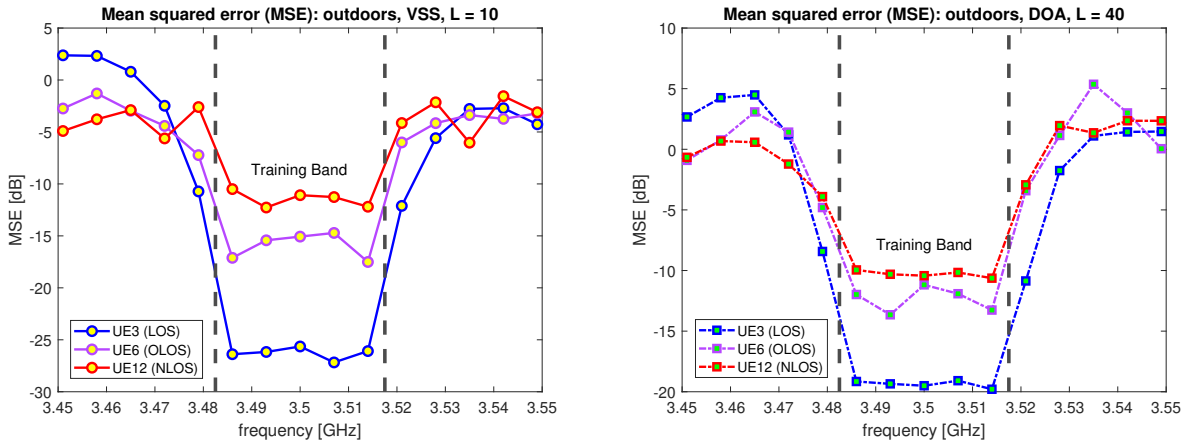

(a) VSS model

(b) DOA model

Fig. 6. Mean squared error (MSE) of estimated/extrapolated channel (outdoors, UE 3/6/12)

based on all models at all locations estimates the channel reasonably well. The best accuracy was achieved for the LOS, followed by the OLOS, and finally the NLOS. Among the VSS and the DOA models, the VSS estimates the channel more accurately even with smaller number of paths because - as explained in section II - the VSS model estimates more parameter values than the DOA model ($2ML + L$ vs $5L$) to improve the fitness to the measured channel data within the training band. Unfortunately, MSE quickly worsens outside the training band for all cases, meaning the extrapolated channel deviates from the measured channel.

However, MSE is not the most practical figure of merit when using channel extrapolation for communication system design purposes. Even if the extrapolated channel is not exactly similar to the measured channel, a communication system may still perform almost as well as if it had the true (measured) channel available. For example, beamforming gain can be robust to errors in the channel estimate. Indeed, in practice, so-called user specific reference signals are embedded in the stream to each user so that they can correct for a potential phase mismatch. This effect is not taken into account by the MSE but well by the beamforming efficiency. Results of beamforming efficiency in Fig. 7 indeed provide alternative views on channel extrapolation. Beamforming efficiencies were averaged per case (4 UEs), using the VSS model (Fig. 7a) and the DOA model (Fig. 7c). Also, the CDF of beamforming efficiencies for all 12 locations (raw values for all UEs, not averaged values), 105 MHz away from the training band (marked in pink in Fig. 7a and 7c), are shown in Fig. 7b and Fig. 7d, with additional results when $L = 1$.

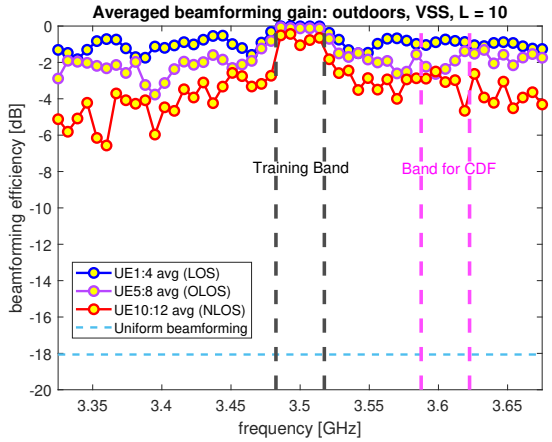

(a) Averaged beamforming efficiency (VSS)

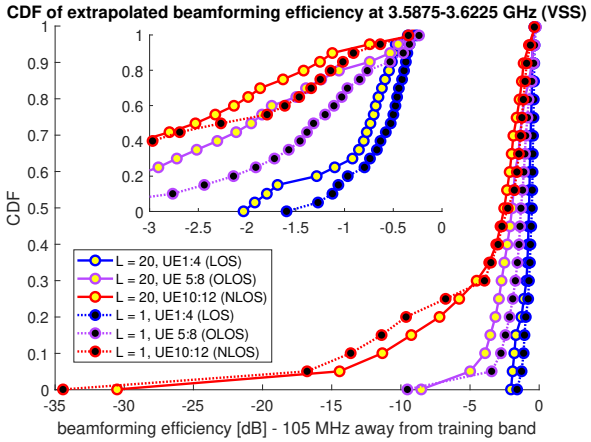

(b) CDF of 12 UEs with varying L (VSS)

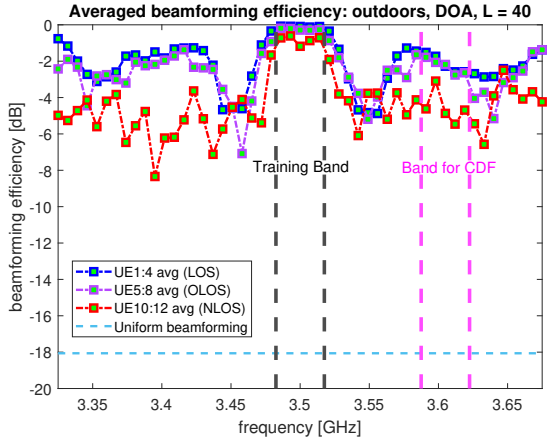

(c) Averaged beamforming efficiency (DOA)

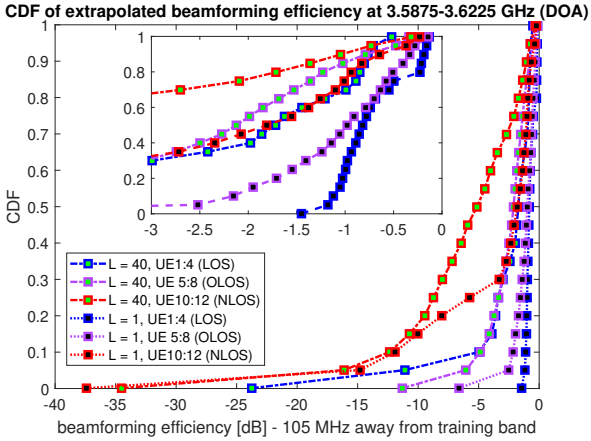

(d) CDF of 12 UEs with varying L (DOA)

Fig. 7. Averaged beamforming efficiency over frequency and CDF of beamforming efficiency (not averaged) 105 MHz away from the training band (outdoors, UE 1:12)

There are several points to be made. First, in general, the DOA model provides higher variance and more deviation from perfect CSI than the VSS model. This may be attributed to 1) imperfect calibration of antenna array and 2) not enough parameters to estimate per MPC. It is therefore more practical to use the VSS model for extrapolation than the DOA model because no calibration data is required, and the computing speed is quicker. Second, regardless of the model, using only one path was usually better (Fig. 7b and Fig. 7d). The outdoor measurements, even in the NLOS case, were better explained with a single path, than with multiple paths. Therefore, choosing many paths possibly resulted in overfitting during the extrapolation. Lastly, while every case outperforms uniform beamforming, the performance decreases in the order of the LOS case, the

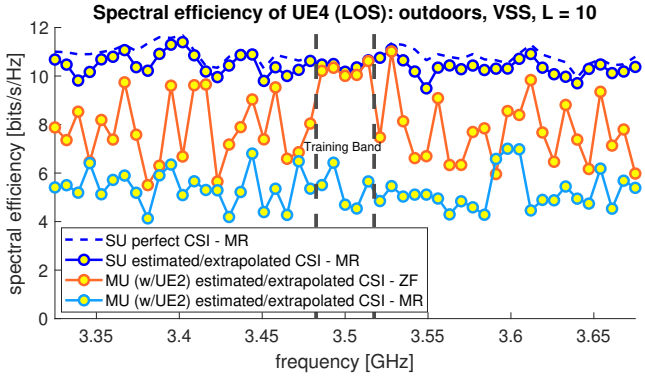

(a) SE for UE4 (LOS)

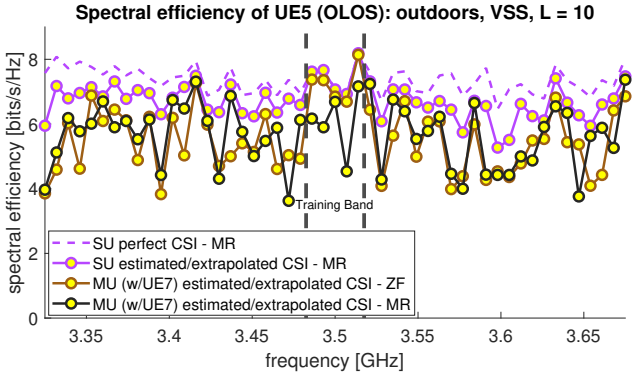

(b) SE for UE5 (OLOS)

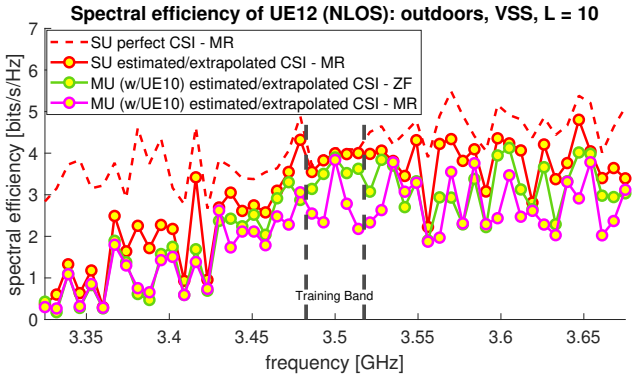

(c) SE for UE12 (NLOS)

Fig. 8. Spectral efficiency comparing single-user/multi-user scenarios with the estimated channels based on the VSS model (outdoors, UE 4/5/12)

OLOS case, then the NLOS case. In Fig. 7b, the LOS performs well, with all beamforming efficiency values greater than -1.5 dB when $L = 1$. For the OLOS case, more than 90 percent of the relative beamforming gain values are greater than -3 dB. In contrast, only 60 percent of the beamforming efficiency was greater than -3 dB for the NLOS case. Overall, in terms of

beamforming efficiency, extrapolation based on HRPE shows potential, especially for the LOS cases where single path dominates the channel.

Shown in Fig. 8 are spectral efficiency plots of both single-user and multi-user systems, achieved with the VSS model using 10 paths (the DOA model was omitted due to lack of space and similar characteristics to the VSS model). For transmit SNR per user n, $\frac{{\sigma_{s(n)}}^2}{{\sigma_{w(n)}}^2} = 10^{10}$ (100 dB) was used based on the assumption that the difference between the transmit power of a BS and a noise floor of a UE is around 105 dB (for example, 35 dBm transmit power from outdoor BS and -70 dBm noise floor of UE). For multi-user scenarios, 2 UEs within the same case (UE 2&4/5&7/10&12) are served together, where 2 UEs were chosen randomly from each LOS/OLOS/NLOS case. Three figures indicate the performances for UE4/5/12 accordingly. Each figure contains four plots. There are single-user performance with perfect CSI (which is also very close to multi-user ZF performance with perfect CSI - not shown on the figure), single-user performance with estimated/extrapolated CSI, multi-user ZF performance with estimated/extrapolated CSI, and multi-user MR performance with estimated/extrapolated CSI.

The results show that extrapolated single-user spectral efficiency matches closely with single-user spectral efficiency based on perfect CSI, while the deviations become larger as we move to the OLOS and then to the NLOS cases. Also, despite using just two users, multi-user scenarios show large deviation from single-user scenario. This indicates that interference exists at the extrapolated frequencies even for well separated users, even though such interference does not exist within the training band. Lastly, ZF performs better than MR in a LOS scenario where the noise power is relatively smaller than the interference power, while they perform relatively similar in OLOS/NLOS scenarios where due to the decrease in signal strength the noise power dominates the SINR value. Overall, in terms of spectral efficiency, extrapolation works best for single-user scenario and when the user is in LOS.

B. 2.4-2.5 and 5-7 GHz Indoor

Next, 2.4-2.5 and 5-7 GHz indoor measurements are analyzed together. 20 MHz between 2.4 and 2.42 GHz was selected as a training band for the first frequency band and 100 MHz between 5 and 5.1 GHz was selected as a training band for the second frequency band. Different variations of the frequency bands were selected to observe the effects of the training band size. Again, SAGE was applied twice for eight BS/UE combinations (2 BS locations and 4 UE locations), based on the VSS and the DOA models. 10 and 60 paths were used respectively.

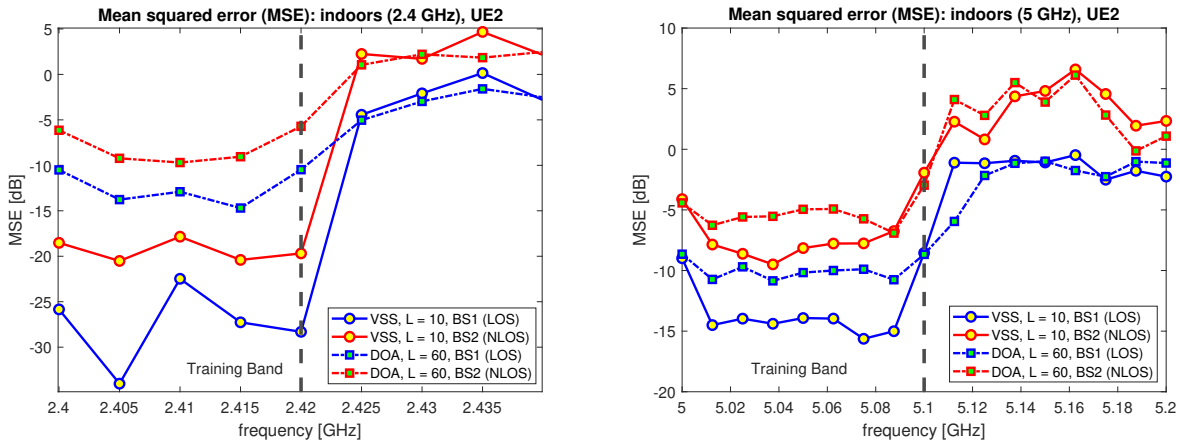

(a) 2.4 GHz case

(b) 5 GHz case

Fig. 9. Mean squared error (MSE) of estimated/extrapolated channel (indoors, UE 2)

In Fig. 9, plots to the left of the black dashed lines show the MSE of the estimated channels in the training bands. UE2 was arbitrarily selected, where it was assumed to be served by BS1 (LOS) or BS2 (NLOS). MSE is below -10 dB for the LOS case for the frequency points within the training band, meaning parameter values estimated by SAGE algorithm could explain the channel accurately with the two channel models provided in section II. However, the NLOS case provided a relatively higher MSE, especially for the 5 GHz case. This is mainly because choosing the most accurate parameters for each MPC becomes difficult especially when the frequency band widens and when the LOS path does not exist. For the frequency points outside the training band, MSE performance degrades quickly. Like the 3.5 GHz outdoor case, the parameter values of MPCs change quickly when moving to another frequency band.

MSE performance again seems to discourage usage of channel extrapolation based on SAGE algorithm. Yet, in Fig. 10, beamforming efficiency shows that channel extrapolation could be useful in the LOS cases. In Fig. 10a and 10c, beamforming efficiency is close to 0 dB for all the LOS cases within the training band, meaning beamforming gain achieved with estimated channel response and the ground truth channel response is very similar. For the NLOS cases within the training band, while the VSS model for the 2.4 GHz case provides very little beamforming loss, other cases result in -1 to -3 dB beamforming efficiency, which can still be acceptable.

Beamforming efficiency outside the training band performs worse for indoors than outdoors. Unlike Fig. 7b and 7d which showed that most extrapolated channels provide -3 dB or greater

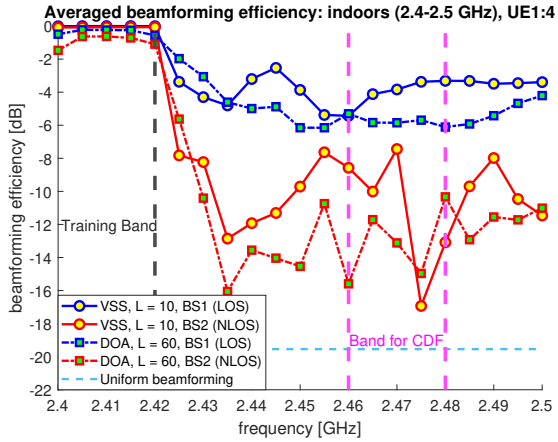

(a) Averaged beamforming efficiency (2.4-2.5 GHz)

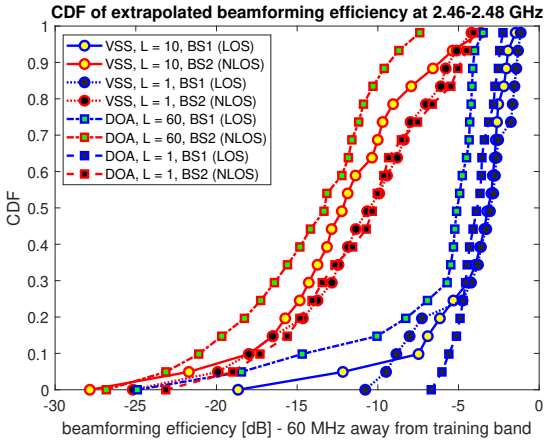

(b) CDF of 4 UEs with varying L (2.46-2.48 GHz)

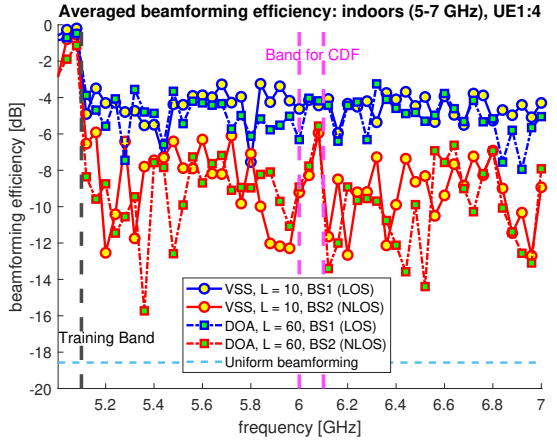

(c) Averaged beamforming efficiency (5-7 GHz)

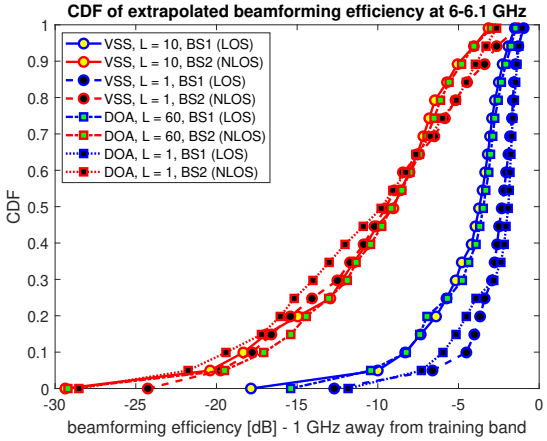

(d) CDF of 4 UEs with varying L (6-6.1 GHz)

Fig. 10. Averaged beamforming efficiency over frequency and CDF of beamforming efficiency (not averaged) 60/1000 MHz away from the training band (indoors, UE 1:4)

beamforming efficiency 105 MHz away from the training band, less than 50 percent of the LOS cases provided greater than -3 dB beamforming efficiency in Fig. 10b and less than 70 percent in Fig. 10d. The figures also showed that one path provided higher beamforming efficiency. This is possibly due to many paths other than the LOS path contributing to the channel in the indoors environment, and the LOS path is best extrapolated. The fact that the large extrapolation range (1.9 GHz) in the 5 GHz case and the beamforming performance do not have clear correlation shows that the LOS path can be extrapolated easily. For the NLOS cases, the beamforming efficiency was generally much worse than the LOS cases, discouraging the use of extrapolation. The results again show difficulty of extrapolation without dominant LOS path and within rich

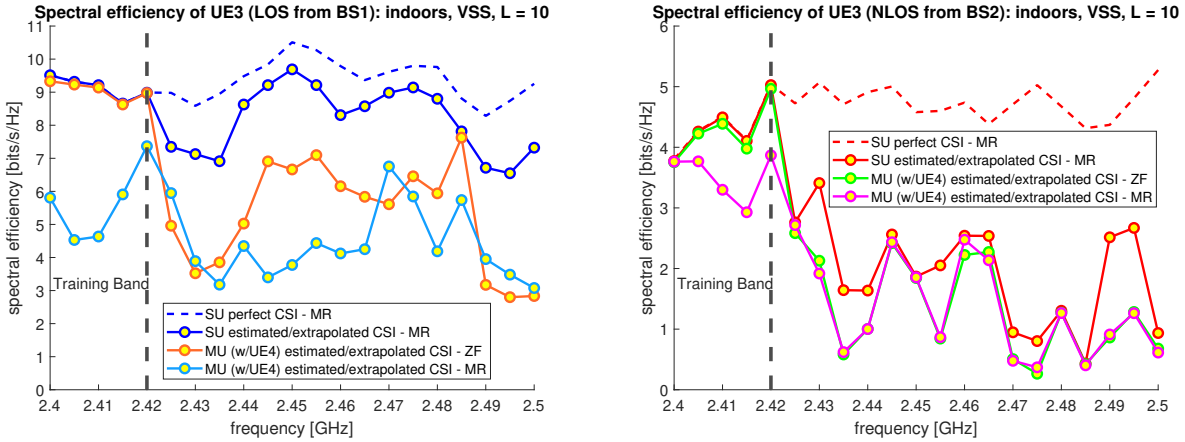

(a) SE for UE3 (LOS)

(b) SE for UE3 (NLOS)

Fig. 11. Spectral efficiency comparing single-user/multi-user scenarios with the estimated channels based on the VSS model (indoors, UE 3)

scattering environment, as theoretically foreseen in [9]. In terms of the model, the VSS model had better performance than the DOA model for the 2.4-2.5 GHz case, while both models had similar performances for the 5-6 GHz case.

Lastly, Fig. 11 shows the spectral efficiency for UE3 served by BS1 (LOS) and BS2 (NLOS). Only the results for the 2.4-2.5 GHz case using the VSS model was plotted due to space restriction and similarity of the DOA results. Just like in Fig. 8, there are two scenarios, where only the UE3 is served (single-user) and where both UE3 and UE4 are served simultaneously (multi-user). Two different precodings, MR and ZF, are used for the multi-user case. For transmit SNR per user n, $\frac{\sigma_{s(n)}{}^2}{\sigma_{w(n)}{}^2} = 10^8$ (80 dB) was used based on the assumption that the difference between the transmit power of a BS and a noise floor of a UE is around 85 dB (for example, 15 dBm transmit power from outdoor BS and -70 dBm noise floor of UE).

The results show that while the single-user performance using extrapolated channels is relatively small for the LOS case (differing by 2 bits/s/Hz at maximum), it does not perform as well as the LOS case in outdoor environment as in Fig. 8a. As expected, the extrapolated channel provides large loss in spectral efficiency for the NLOS case. For the NLOS case, single-user performance and the multi-user performance are rather similar in the extrapolated bands. While ZF provides better than MR for the LOS case, they are overlapping for the NLOS case. Overall, extrapolation is difficult in multi-user scenarios, especially in the NLOS case, while it performs relatively better for single-user scenarios in LOS case.

VI. Conclusion

To eliminate large overheads in the FDD massive MIMO systems, an experimental study of the feasibility of channel extrapolation using parameters of MPCs at a selected training frequency band attained by HRPE algorithm to estimate the channel frequency response at a desired frequency band was presented. Empirical data obtained by three massive MIMO channel measurement setups in outdoor and indoor environments were used for verification.

The results showed that the best extrapolation performance can be achieved when 1) a channel contains a dominant LOS path, 2) the BS is not surrounded by interacting objects (outdoor), and 3) UEs are well separated. One of the reasons why the extrapolation in the NLOS cases is difficult is because small-scale fading is less predictable. Another source of error may be simplicity of the channel model, which assumes MPCs to be planar waves with perfect vertical polarization. Such model assumption will not hold when BS is too close to interacting objects. Therefore, the suggested extrapolation method will perform best in the FDD massive MIMO systems that follow conditions 1)-3). We conjecture that a particularly appealing case could be channels in stationary unmanned aerial vehicle (UAV) communication systems which usually involve high LOS probability, outdoor environment, well separated aerial vehicles, and long enough channel coherence time. The FDD massive MIMO systems for terrestrial applications involving mainly NLOS cases, however, may still require at least partial downlink pilot and feedback overheads or better extrapolation techniques in order to improve performance.

Another notable result was that extrapolation based on a simpler VSS model, which estimates an abstract antenna array pattern, performs better than extrapolation based on the DOA model, which uses measured calibration data of antenna array to find arriving directions of MPCs. This is somewhat counter-intuitive: more knowledge about the antenna array used during the measurement would be expected to provide better results, but the opposite occurs. One possible explanation is the sensitivity to calibration and model errors. If the goal of HRPE is reconstructing an estimated channel based on observation rather than finding angular characteristics of MPCs, the VSS might thus be a preferable algorithm.

Several topics arising from the current work will be considered in the future, including: 1) extrapolation performance dependence on number and/or geometry (planar or cylindrical) of antennas at BS and/or UEs, 2) extension and/or improvement of channel model including polarization parameter and/or spherical wave model, and 3) channel measurements between a

drone and an antenna array to verify HRPE based channel extrapolation techniques for a realistic massive MIMO system dominated by LOS path.

APPENDIX A
SAGE ALGORITHM

The SAGE algorithm, explained in [11], identifies "the estimated parameters describing MPCs in a channel", $\hat{\mathbf{\Psi}}$, maximizing the likelihood of "the observed complex channel frequency response", $H(m, f_k)$, over all antennas (with index m) and frequency points (with index k):

$$\hat{\mathbf{\Psi}} = \arg\min_{\hat{\mathbf{\Psi}}} \sum_{m} \sum_{k} |H(m, f_k) - \hat{H}(m, f_k; \hat{\mathbf{\Psi}})|^2.$$

$\hat{H}(m, f_k; \hat{\mathbf{\Psi}})$ is "the estimated complex channel frequency response" related to $\hat{\mathbf{\Psi}} = (\hat{\boldsymbol{\psi}}_1, \ldots, \hat{\boldsymbol{\psi}}_L)$, where L is the total number of paths in a channel, through the VSS or the DOA models previously introduced in section II.

This optimization problem is challenging because of 1) the high-dimensionality scaling with L and 2) the non-linear dependence on the path parameters. The SAGE algorithm provides an efficient suboptimal solution to the problem of relying on an iterative approach.

Fig. 12 is the SAGE algorithm flow chart. The estimates of "the ground truth parameters", $\mathbf{\Psi}$, at iteration μ, are denoted by $\hat{\mathbf{\Psi}}(\mu)$. Successive ordered cancellation is used to estimate initial parameters, $\hat{\mathbf{\Psi}}(0)$, as explained in [11]. At each iteration, only the parameters corresponding to one path, *e.g.*, $\hat{\boldsymbol{\psi}}_v$ *or* $\hat{\boldsymbol{\psi}}_d$, are optimized while parameters for other paths keep their past value. Optimizing parameters per path reduces the search dimensions by a factor L. A set of L iterations, called an iteration cycle, is required to update the parameters for each of the L paths. After an iteration cycle, each path is re-estimated based on the updated values of other paths.

Each iteration consists of two steps: 1) expectation step and 2) maximization step. The specific operations performed in the two steps for the VSS and the DOA algorithms are shown in Fig. 13. During the expectation step, the interference due to other paths is canceled from the measured channel response based on their current estimate. Then, during the maximization step, the parameters $\hat{\boldsymbol{\psi}}_v$ or $\hat{\boldsymbol{\psi}}_d$ are re-estimated. To further simplify the complexity of the problem, the optimization over the different parameters of each path is simplified into several one-dimensional searches optimizing each parameter at a time. The algorithm iterates until convergence or if a maximal number of iterations is achieved.

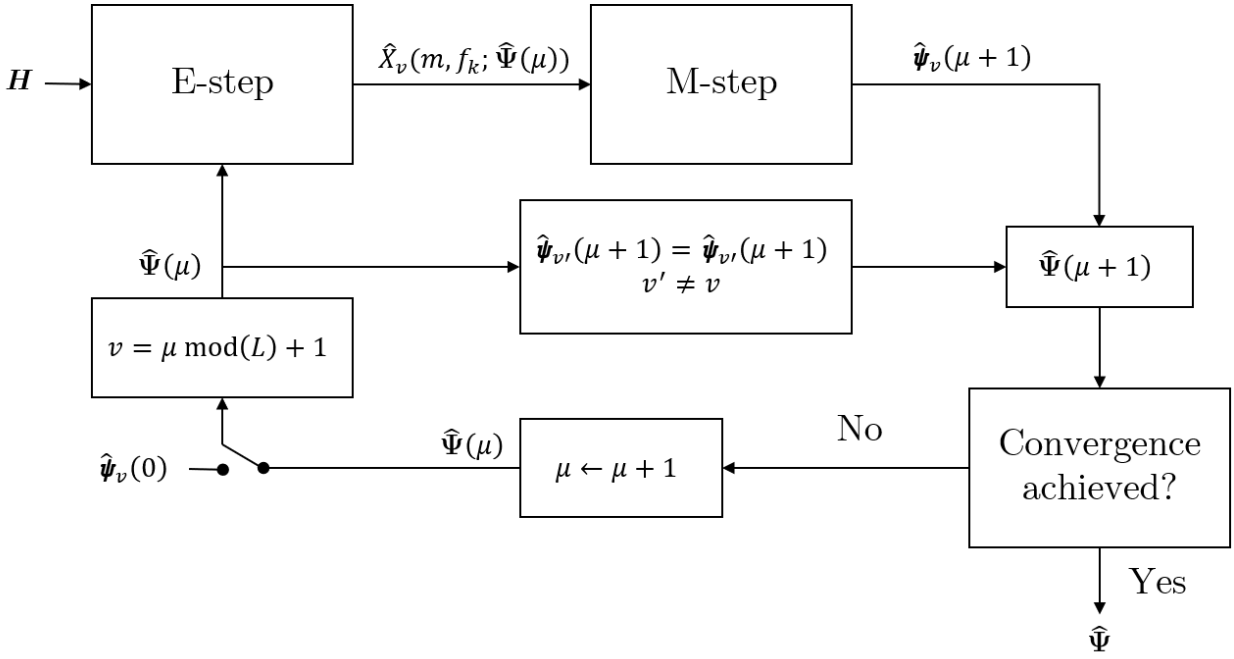

Fig. 12. SAGE algorithm flow graph for the VSS model - v can be replaced by d for the DOA model

	VSS	DOA
Path parameters $\boldsymbol{\Psi} = (\boldsymbol{\psi}_1, \ldots, \boldsymbol{\psi}_L)$	$\boldsymbol{\psi}_v = (\mathbf{a}_v, \tau_v)$	$\boldsymbol{\psi}_d = (\alpha_d, \tau_d, \phi_d, \theta_d)$
Initialization	Successive ordered cancellation	
Expectation-step (E-step)	$\hat{X}_v(m,f_k;\hat{\Psi}) = H(m,f_k) - \sum_{v'=1,v'\neq v}^{L} \hat{\mathrm{a}}_{v'}(m) e^{-j2\pi f_k \hat{\tau}_{v'}}$	$\hat{X}_d(m,f_k;\hat{\Psi}) = H(m,f_k) - \sum_{d'=1,d'\neq d}^{L} \hat{\alpha}_{d'} A(m,f_k,\hat{\phi}_{d'},\hat{\theta}_{d'}) e^{-j2\pi f_k \hat{\tau}_{d'}}$
Maximization-step (M-step)	$\hat{\tau}_v = \arg\max_{\tau} \sum_m \left\| \sum_k \hat{X}_v(m,f_k;\hat{\Psi}) e^{j2\pi f_k \tau_v} \right\|^2$ $\hat{\mathrm{a}}_v(m) = \frac{1}{K} \sum_k \hat{X}_v(m,f_k;\hat{\Psi}) e^{j2\pi f_k \hat{\tau}_v}$	$(\hat{\tau}_d, \hat{\phi}_d, \hat{\theta}_d) = \arg\max_{\tau_d,\phi_d,\theta_d} \frac{\lvert z(\tau_d,\phi_d,\theta_d)\rvert^2}{P(\phi_d,\theta_d)}$, $\hat{\alpha}_d = \frac{z(\hat{\tau}_d,\hat{\phi}_d,\hat{\theta}_d)}{P(\hat{\phi}_d,\hat{\theta}_d)}$ $z(\tau_d,\phi_d,\theta_d) = \sum_m \sum_k \hat{X}_d(m,f_k;\hat{\Psi}) \overline{A(m,f_k,\phi_d,\theta_d)} e^{j2\pi f_k \tau_d}$ $P(\phi_d,\theta_d) = \sum_m \sum_k \lvert A(m,f_k,\phi_d,\theta_d)\rvert^2$

Fig. 13. Descriptions of SAGE algorithm steps for the VSS and the DOA models

ACKNOWLEDGMENT

The authors would like to thank A. Adame, A. Alvarado, Z. Cheng, Dr. C. U. Bas, Dr. N. Abbasi, and Dr. D. Burghal for help with channel sounder development, measurement campaigns, and productive technical discussions.

REFERENCES

[1] T. Choi, F. Rottenberg, J. Gomez-Ponce, A. Ramesh, P. Luo, J. Zhang, and A. F. Molisch, "Channel Extrapolation for FDD Massive MIMO: Procedure and Experimental Results," in *2019 IEEE 90th Vehicular Technology Conference (VTC2019-Fall)*, Sep. 2019, pp. 1–6.

[2] T. L. Marzetta, "Noncooperative Cellular Wireless with Unlimited Numbers of Base Station Antennas," *IEEE Transactions on Wireless Communications*, vol. 9, no. 11, pp. 3590–3600, November 2010.

[3] T. L. Marzetta, E. G. Larsson, H. Yang, and H. Q. Ngo, *Fundamentals of Massive MIMO*. Cambridge University Press, 2016.

[4] E. Björnson, J. Hoydis, and L. Sanguinetti, "Massive MIMO Networks: Spectral, Energy, and Hardware Efficiency," *Foundations and Trends® in Signal Processing*, vol. 11, no. 3-4, pp. 154–655, 2017. [Online]. Available: http://dx.doi.org/10.1561/2000000093

[5] E. Björnson, E. G. Larsson, and T. L. Marzetta, "Massive MIMO: ten myths and one critical question," *IEEE Communications Magazine*, vol. 54, no. 2, pp. 114–123, February 2016.

[6] J. Flordelis, F. Rusek, F. Tufvesson, E. G. Larsson, and O. Edfors, "Massive MIMO Performance—TDD Versus FDD: What Do Measurements Say?" *IEEE Transactions on Wireless Communications*, vol. 17, no. 4, pp. 2247–2261, April 2018.

[7] 3GPP, "Evolved Universal Terrestrial Radio Access (E-UTRA); User Equipment (UE) radio transmission and reception," 3rd Generation Partnership Project (3GPP), Technical Specification (TS) 36.101, October 2019, version 16.3.0.

[8] F. Rottenberg, R. Wang, J. Zhang, and A. F. Molisch, "Channel Extrapolation in FDD Massive MIMO: Theoretical Analysis and Numerical Validation," in *2019 IEEE Global Communications Conference (GLOBECOM)*, Dec 2019, pp. 1–7.

[9] F. Rottenberg, T. Choi, P. Luo, J. Zhang, and A. F. Molisch, "Performance Analysis of Channel Extrapolation in FDD Massive MIMO Systems," *IEEE Transactions on Wireless Communications*, pp. 1–1, 2020.

[10] M. D. Larsen, A. L. Swindlehurst, and T. Svantesson, "Performance Bounds for MIMO-OFDM Channel Estimation," *IEEE Transactions on Signal Processing*, vol. 57, no. 5, pp. 1901–1916, May 2009.

[11] B. H. Fleury, M. Tschudin, R. Heddergott, D. Dahlhaus, and K. Ingeman Pedersen, "Channel parameter estimation in mobile radio environments using the SAGE algorithm," *IEEE Journal on Selected Areas in Communications*, vol. 17, no. 3, pp. 434–450, March 1999.

[12] X. Rao and V. K. N. Lau, "Distributed Compressive CSIT Estimation and Feedback for FDD Multi-User Massive MIMO Systems," *IEEE Transactions on Signal Processing*, vol. 62, no. 12, pp. 3261–3271, June 2014.

[13] J. Choi, D. J. Love, and P. Bidigare, "Downlink Training Techniques for FDD Massive MIMO Systems: Open-Loop and Closed-Loop Training With Memory," *IEEE Journal of Selected Topics in Signal Processing*, vol. 8, no. 5, pp. 802–814, Oct 2014.

[14] Z. Gao, L. Dai, Z. Wang, and S. Chen, "Spatially Common Sparsity Based Adaptive Channel Estimation and Feedback for FDD Massive MIMO," *IEEE Transactions on Signal Processing*, vol. 63, no. 23, pp. 6169–6183, Dec 2015.

[15] A. Adhikary, J. Nam, J. Ahn, and G. Caire, "Joint Spatial Division and Multiplexing—The Large-Scale Array Regime," *IEEE Transactions on Information Theory*, vol. 59, no. 10, pp. 6441–6463, Oct 2013.

[16] Z. Jiang, A. F. Molisch, G. Caire, and Z. Niu, "Achievable Rates of FDD Massive MIMO Systems With Spatial Channel Correlation," *IEEE Transactions on Wireless Communications*, vol. 14, no. 5, pp. 2868–2882, May 2015.

[17] H. Xie, F. Gao, S. Zhang, and S. Jin, "A Unified Transmission Strategy for TDD/FDD Massive MIMO Systems With Spatial Basis Expansion Model," *IEEE Transactions on Vehicular Technology*, vol. 66, no. 4, pp. 3170–3184, April 2017.

[18] H. Liang, W. Chung, and S. Kuo, "FDD-RT: A Simple CSI Acquisition Technique via Channel Reciprocity for FDD Massive MIMO Downlink," *IEEE Systems Journal*, vol. 12, no. 1, pp. 714–724, March 2018.

[19] W. Shen, L. Dai, B. Shim, Z. Wang, and R. W. Heath, "Channel Feedback Based on AoD-Adaptive Subspace Codebook in FDD Massive MIMO Systems," *IEEE Transactions on Communications*, vol. 66, no. 11, pp. 5235–5248, Nov 2018.

[20] M. Alrabeiah and A. Alkhateeb, "Deep Learning for TDD and FDD Massive MIMO: Mapping Channels in Space and Frequency," *arXiv e-prints*, p. arXiv:1905.03761, May 2019.

[21] Y. Liao, H. Yao, Y. Hua, and C. Li, "CSI Feedback Based on Deep Learning for Massive MIMO Systems," *IEEE Access*, vol. 7, pp. 86 810–86 820, 2019.

[22] Y. Yang, F. Gao, G. Y. Li, and M. Jian, "Deep Learning-Based Downlink Channel Prediction for FDD Massive MIMO System," *IEEE Communications Letters*, vol. 23, no. 11, pp. 1994–1998, Nov 2019.

[23] M. Pun, A. F. Molisch, P. Orlik, and A. Okazaki, "Super-Resolution Blind Channel Modeling," in *2011 IEEE International Conference on Communications (ICC)*, June 2011, pp. 1–5.

[24] W. Yang, L. Chen, and Y. E. Liu, "Super-Resolution for Achieving Frequency Division Duplex (FDD) Channel Reciprocity," in *2018 IEEE 19th International Workshop on Signal Processing Advances in Wireless Communications (SPAWC)*, June 2018, pp. 1–5.

[25] U. Ugurlu, R. Wichman, C. B. Ribeiro, and C. Wijting, "A Multipath Extraction-Based CSI Acquisition Method for FDD Cellular Networks With Massive Antenna Arrays," *IEEE Transactions on Wireless Communications*, vol. 15, no. 4, pp. 2940–2953, April 2016.

[26] X. Zhang, L. Zhong, and A. Sabharwal, "Directional Training for FDD Massive MIMO," *IEEE Transactions on Wireless Communications*, vol. 17, no. 8, pp. 5183–5197, Aug 2018.

[27] H. Krim and M. Viberg, "Two decades of array signal processing research: the parametric approach," *IEEE Signal Processing Magazine*, vol. 13, no. 4, pp. 67–94, July 1996.

[28] N. Jalden, H. Asplund, and J. Medbo, "Channel extrapolation based on wideband MIMO measurements," in *2012 6th European Conference on Antennas and Propagation (EUCAP)*, March 2012, pp. 442–446.

[29] J. Medbo and F. Harrysson, "Efficiency and accuracy enhanced super resolved channel estimation," in *2012 6th European Conference on Antennas and Propagation (EUCAP)*, March 2012, pp. 16–20.

[30] D. Vasisht, S. Kumar, H. Rahul, and D. Katabi, "Eliminating Channel Feedback in Next-Generation Cellular Networks," in *Proceedings of the 2016 ACM SIGCOMM Conference*, ser. SIGCOMM '16. New York, NY, USA: ACM, 2016, pp. 398–411. [Online]. Available: http://doi.acm.org/10.1145/2934872.2934895

[31] M. Arnold, S. Dörner, S. Cammerer, S. Yan, J. Hoydis, and S. ten Brink, "Enabling FDD Massive MIMO through Deep Learning-based Channel Prediction," 2019.

[32] J. Hong, J. Rodríguez-Piñeiro, and X. Yin, "FDD Channel Inference Methods With Experimental Performance Evaluation," *IEEE Access*, vol. 8, pp. 10 491–10 502, 2020.

[33] R. Schmidt, "Multiple emitter location and signal parameter estimation," *IEEE Transactions on Antennas and Propagation*, vol. 34, no. 3, pp. 276–280, March 1986.

[34] R. Roy and T. Kailath, "ESPRIT-estimation of signal parameters via rotational invariance techniques," *IEEE Transactions on Acoustics, Speech, and Signal Processing*, vol. 37, no. 7, pp. 984–995, July 1989.

[35] J. A. Hogbom, "Aperture Synthesis with a Non-Regular Distribution of Interferometer Baselines," *Astron. Astrophys. Suppl. Ser.*, vol. 15, pp. 417–426, 1974.

[36] A. Richter, *Estimation of Radio Channel Parameters: Models and Algorithms*. ISLE, 2005. [Online]. Available: https://books.google.com/books?id=XZEVMQAACAAJ

[37] M. Friese, "Multitone signals with low crest factor," *IEEE Transactions on Communications*, vol. 45, no. 10, pp. 1338–1344, Oct 1997.